Coordination Chemistry of the Nitronyl and Imino Nitroxides. Linear Chain Adducts with Rhodium(II) Trifluoroacetate Dimer[1]

Andre Cogne, Andre Grand, Paul Rey,* and Robert Subra

Contribution from the Laboratoires de Chimie, (U.A., C.N.R.S. 1194), Département de Recherche fondamentale, Centre d'Etude Nucléaires, 38041 Grenoble Cédex, France.
Received August 9, 1988

Abstract: The nitronyl and imino nitroxides (2-phenyl-4,4,5,5-tetramethyl-4,5-dihydro-1*H*-imidazolyl-1-oxy 3-oxide (NITPh), 2,4,4,5,5-pentamethyl-4,5-dihydro-1*H*-imidazolyl-1-oxy 3-oxide (NITMe), 2,4,4,5,5-pentamethyl-4,5-dihydro-1*H*-imidazolyl-1-oxy (IMMe)) react with tetrakis(trifluoroacetato)dirhodium(II) ($Rh_2(tfac)_4$) resulting in adducts which are bisnitroxyl complexes or extended linear chains of alternating organic free radicals and metal fragments. Structural data for these adducts are as follows: $Rh_2(tfac)_4 \cdot (NITPh)_2$, **1**, space group $P\bar{1}$, a = imino nitroxides. (1) Å, b = 10.529 (1) Å, c = 14.175 (1) Å, α = 73.71 (1)°, β = 77.23 (1)°, γ = 80.23 (1)°, Z = 1; $Rh_2(tfac)_4 \cdot NITMe$, **2**, space group $P2_1/n$, a = 11.917 (1) Å, b = 16.220 (2) Å, c = 14.402 (2) Å, β = 100.24 (1)°, Z = 2; $Rh_2(tfac)_4 \cdot IMMe_2$, **3**, space group $I4_1/a$, a = 23.850 (2) Å, b = 23.850 (2) Å, c = 12.636 (1) Å, Z = 8; $Rh_2(tfac)_4 \cdot IMMe$, **4**, space group $P2_1/c$, a = 8.614 (1) Å, b = 17.800 (2) Å, c = 18.133 (2) Å, β = 98.65 (1)°, Z = 4. Both compounds **1** and **3** are centrosymmetric bis-adducts containing respectively axial O-bonded nitronyl nitroxides and *N*-bonded imino nitroxides. On the other hand compounds **2** and **4** are extended chains of nitroxides bridged by metal fragments. Magnetic data were obtained for the four compounds between 6 and 300 K and were interpreted using the models derived from the structural results. The O-bonded adducts, **1** and **2**, exhibit fairly large antiferromagnetic interactions (−167 and −197 cm^{-1}), while the N-bonded adducts, **3** and **4**, display weak (positive or negative, −11 and +4 cm^{-1}) internitroxide couplings. Extended Hückel calculations show that this difference is not the consequence of different electronic structures for the nitronyl and the imino nitroxides. Furthermore, the analysis of the short contacts in the X-ray structures demonstrates that the internitroxyl coupling is mediated by the Rh–Rh bond. On the basis of local symmetry considerations, it is proposed that this mediation mainly involves a metal fragment orbital of σ symmetry. It is possible, considering this σ mechanism, to make a quantitative comparison of the magnitude of the coupling constants in two of the complexes. Finally, an EHT calculation on compound **1** shows that the SOMO of each nitroxide does indeed interact mainly with the σ and the σ^* orbitals of the rhodium dimer moiety.

In recent years, much interest has been devoted to magneto-structural correlations in transition-metal complexes, particularly to low-dimensional magnetic systems.[2] The synthesis of such systems is a challenging problem since the low dimensionality in the solid state depends, to a large extent, on stacking constraints which are not controlled processes. One approach to this problem is to use bidentate bridging ligands in order to enforce a "polymeric" structure on the molecular scale. The magnetic properties of such systems will depend on the ability of the bridging ligand to propagate the magnetic information over the entire molecular framework.

Extensive data on species in which paramagnetic transition metals are bridged by diamagnetic organic fragments are available.[2] On the other hand, no work has been devoted as yet to the reverse situation in which an organic free radical bridges diamagnetic metal systems. This is surprising since it is anticipated that such molecular frameworks would give information regarding the electronic structure of the metal fragment and could lead to new magnetic materials. We present here a study of the adducts obtained by reacting the diamagnetic rhodium(II) trifluoroacetate dimer, ($Rh(tfac)_4$), with bidentate nitroxyl free radicals.

Although generally monodentate, the nitroxyl free radicals have been the subject of intense interest, since some of the oligonuclear complexes with transition-metal ions show unusual magnetic properties. One example deserves special mention. In (4-hydroxy-2,2,6,6-tetramethylpiperidinyl-1-oxy)bis(hexafluoroacetylacetonato)copper(II) ($Cu(hfac)_2$Tempol) both the oxy and the hydroxy groups are coordinated, leading to a chain structure in the solid state.[3] The magnetic data are consistent with a weak interaction mediated by the saturated carbon framework linking the two coordinated groups.[4,5] This example showed that suitably functionalized nitroxyl free radicals might be used as bridging paramagnetic ligands.

Notable among the stable free radicals are the nitronyl[6] and the imino nitroxides[7] (Figure 1). The former have two equivalent NO groups linked by an unsaturated organic backbone on which the unpaired electron is equally delocalized, while in the latter the unpaired spin is inequally distributed on the nitroxyl and the imino groups. Both are potential bridging ligands, and a good propagation of the magnetic information is expected. Extended linear chains of alternating paramagnetic transition-metal ions and nitronyl nitroxides have indeed been prepared and characterized;[8,9] the exceptional magnetic properties of these adducts have prompted us to develop our study of the coordination properties of these free radicals toward other metal systems.

The choice of the dirhodium tetracarboxylate system as a metal-containing bridging group to prepare chains of organic free radicals was based mainly on the following two reasons. First, this system is diamagnetic but able to propagate magnetic interactions;[10,11] second, the nature of the carboxylate ligands is such that they offer minimal steric hindrance, and, as observed for Tempo, bulky axial ligands can be accommodated without

(1) A preliminary account of this work has been reported: Cogne, A.; Grand, A.; Rey, P.; Subra, R. *J. Am. Chem. Soc.* **1987**, *109*, 7927–7929.
(2) For reviews, see: (a) *Magneto-Structural Correlations in Exchange Coupled Systems*; Willett, R. D., Gatteschi, D., Kahn, O., Eds.; D. Reidel: Dordrecht, Holland, 1985. (b) *Extended Linear Chain Compounds*; Miller, J. S., Ed.; Plenum Press: New York, 1983. (c) *Organic and Inorganic Low Dimensional Crystalline Materials*; Delhaes, P., Drillon, M., Eds.; NATO ASI; Plenum Press: New York, 1987.
(3) Anderson, O. P.; Kuechler, T. C. *Inorg. Chem.* **1980**, *19*, 1417–1423.
(4) Bencini, A.; Benelli, C.; Gatteschi, D.; Zanchini, C. *J. Am. Chem. Soc.* **1984**, *106*, 5813–5818.
(5) Benelli, C.; Gatteschi, D.; Carnegie, D. W.; Carlin, R. L. *J. Am. Chem. Soc.* **1985**, *107*, 2560–2561.
(6) Ullman, E. F.; Osiecki, J. H.; Boocock, D. G. B.; Darcy, R. *J. Am. Chem. Soc.* **1972**, *94*, 7049–7059.
(7) Ullman, E. F.; Call, L.; Osiecki, J. H. *J. Org. Chem.* **1970**, *35*, 3623–3631.
(8) Caneschi, A.; Gatteschi, D.; Laugier, J.; Rey, P. *J. Am. Chem. Soc.* **1987**, *109*, 2191–2192.
(9) Caneschi, A.; Gatteschi, D.; Rey, P.; Sessoli, R. *Inorg. Chem.*, in press.

0002-7863/89/1511-3230$01.50/0

Table I. Crystallographic Data for Complexes **1–4**

	1	2	3	4
chemical formula	$C_{40}H_{40}F_{12}N_4O_{12}Rh_2$	$C_{16}H_{15}F_{12}N_2O_{10}Rh_2$	$C_{24}H_{30}F_{12}N_4O_{10}Rh_2$	$C_{16}H_{15}F_{12}N_2O_9Rh_2$
molecular wt	1202.82	829.22	968.57	816.22
space group	$P\bar{1}$	$P2_1/n$	$I4_1/a$	$P2_1/c$
a	8.389 (1) Å	11.917 (1) Å	23.850 (2) Å	8.614 (2) Å
b	10.529 (1) Å	16.220 (2) Å	23.850 (2) Å	17.800 (1) Å
c	14.175 (1) Å	14.402 (2) Å	12.636 (1) Å	18.133 (2) Å
α	73.71 (1)°	90.0°	90.0°	90.0°
β	77.23 (1)°	100.24 (1)°	90.0°	98.65 (1)°
γ	80.23 (1)°	90.0°	90.0°	90.0°
V	1164.34 Å^3	2739.48 Å^3	7187.64 Å^3	2748.77 Å^3
Z	1	4	8	4
ρ(calcd)	1.716 g/cm^3	2.001 g/cm^3	1.790 g/cm^3	1.973 g/cm^3
T	20 °C	20 °C	20 °C	20 °C
R	0.034	0.044	0.037	0.039
R_w	0.038	0.051	0.034	0.029

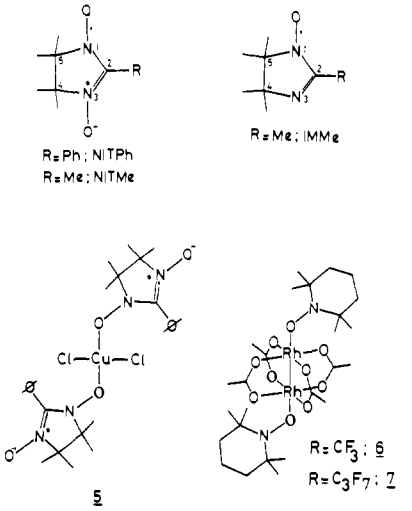

Figure 1. Chemical structures of NITPh, NITMe, IMMe, $Cu(hfac)_2$·$(NITPh)_2$, $Rh_2(tfac)_4$·$(Tempo)_2$, and $Rh_2(hfbu)_4$·$(Tempo)_2$.

crowding complications. Therefore, complexation with the nitronyl and imino nitroxides was expected, and different molecular structures and internitroxyl interactions were anticipated, depending on the nitroxide used. This study confirms the ability of the rhodium–rhodium bond to mediate a sizeable internitroxyl magnetic interaction[10,11] and demonstrates that this mediation mainly involves a metal-fragment orbital of σ symmetry.

Experimental Section

Syntheses. 2-Phenyl-4,4,5,5-tetramethyl-4,5-dihydro-1*H*-imidazolyl-1-oxy 3-oxide (NITPh),[6] 2,4,4,5,5-pentamethyl-4,5-dihydro-1*H*-imidazolyl-1-oxy 3-oxide (NITMe),[6] 2,4,4,5,5-pentamethyl-4,5-dihydro-1*H*-imidazolyl-1-oxy (IMMe),[7] and tetrakis(trifluoroacetato)dirhodium(II) ($Rh_2(tfac)_4$),[12] were prepared according to previously reported procedures.

Synthesis of $Rh_2(tfac)_4$·$(NITPh)_2$, 1. To a solution of $Rh_2(tfac)_4$, (350 mg, 0.53 10^{-3} m) in 20 mL of dry benzene was added a solution of NITPh (260 mg, 1.12 × 10^{-3} m) in the same solvent. Precipitation of dark blue crystals immediately occurred. These were filtered, vacuum dried, and recrystallized from a 2:1 benzene–acetone mixture (560 mg, 87%). Elemental analysis showed that the crude compound as well as the recrystallized product were benzene solvates ($C_{34}H_{34}F_{12}N_4O_{12}Rh_2$, C_6H_6 Calcd: C, 39.94; H, 3.35; F, 18.95; N, 4.68; O, 15.96; Rh, 17.11. Found: C, 39.52; H, 3.06; F, 18.59; N, 4.34, Rh, 17.59).

The other three adducts were prepared with the same procedure and the appropriate proportion of the appropriate free radical and were recrystallized from the same solvent mixture. $Rh_2(tfac)_4$·NITMe, **2**, (69%) ($C_{16}H_{15}F_{12}N_2O_{10}Rh_2$ Calcd: C, 23.18; H, 1.82; F, 27.49; N, 3.39; O, 19.29; Rh, 24.82. Found: C, 23.39; H, 1.80; F, 27.81; N, 3.30; Rh, 24.43). $Rh_2(tfac)_4$·$(IMMe)_2$, **3** (47%) ($C_{24}H_{30}F_{12}N_4O_{10}Rh_2$ Calcd: C, 29.76; H, 3.12; F, 23.54; N, 5.81; O, 16.52; Rh, 21.25. Found: C, 29.44; H, 2.96; F, 23.19; N, 5.75, Rh, 21.06). $Rh_2(tfac)_4$·IMMe, **4** (58%) ($C_{16}H_{15}F_{12}N_2O_9Rh_2$ Calcd C, 23.63; H, 1.86; F, 28.03; N, 3.46; O, 17.17; Rh, 25.31. Found: C, 23.41; H, 1.78; F, 27.85; N, 3.42; Rh, 24.86).

Crystals suitable for an X-ray diffraction study were obtained for the four adducts.

X-ray Data Collection and Reduction. For all compounds the data were obtained from regularly shaped crystals of approximate dimensions 0.20 × 0.20 × 0.20 mm.

Preliminary Weissenberg photographs showed triclinic symmetry for **1**, monoclinic for **2** and **4**, and quadratic for **3**. The space groups $P2_1/n$ for **2**, $I4_1/a$ for **3**, and $P2_1/c$ for **4** were deduced from systematic absences.

The same crystals were mounted on an Enraf-Nonius CAD-4 four-circle diffractometer, and X-ray data were collected with monochromatized Mo Kα radiation. Accurate cell constants were derived from least-squares refinement of the setting angles of 25 reflections and are reported in Table I with other experimental parameters. The data were

Table II. Positional Parameters (×10^4) for Compound **1**, $Rh_2(tfac)_4(NITPh)_2$

	x	y	z	B_{eq}
Rh1	493 (0)	34 (0)	−872 (0)	2.67
O1	1588 (3)	−1851 (3)	−425 (2)	3.53
O2	−1551 (3)	−773 (3)	−846 (2)	3.73
O3	−650 (4)	1930 (3)	−1212 (2)	3.68
O4	2477 (3)	847 (3)	9211 (2)	3.87
C1	1367 (5)	−2407 (4)	485 (4)	3.50
C2	1964 (7)	−3886 (5)	770 (4)	4.61
C3	2506 (5)	1073 (5)	33 (4)	3.63
C4	3861 (7)	1895 (6)	4 (4)	4.73
F1	2231 (8)	−4341 (4)	1639 (3)	12.77
F2	3329 (6)	−4185 (4)	201 (3)	11.90
F3	982 (7)	−4557 (4)	645 (5)	14.06
F4	5283 (3)	1508 (3)	−514 (2)	6.63
F5	3471 (4)	3134 (3)	−456 (3)	8.36
F6	4111 (5)	1838 (5)	881 (2)	10.32
O5	−8812 (4)	174 (3)	−2514 (2)	3.83
O6	−3756 (5)	−1561 (4)	−3996 (3)	7.98
N1	−7638 (5)	−632 (4)	−2888 (2)	3.73
N2	−5254 (5)	−1462 (4)	−3579 (3)	4.84
C5	−6053 (6)	−429 (5)	−3178 (3)	3.77
C6	−8048 (6)	−1757 (5)	−3234 (3)	4.19
C7	−6326 (7)	−2550 (5)	−3373 (4)	4.66
C8	−8686 (8)	−1069 (6)	−4201 (4)	5.58
C9	−9346 (7)	−2497 (6)	−2458 (4)	5.60
C10	−5948 (8)	−3165 (6)	−4272 (4)	6.49
C11	−5918 (8)	−3556 (6)	−2436 (4)	6.15
C12	−5302 (6)	669 (5)	−3106 (3)	3.90
C13	−3650 (7)	505 (6)	−3018 (4)	4.93
C14	−2940 (8)	1571 (7)	−2970 (4)	6.16
C15	6129 (10)	2793 (7)	−3022 (5)	6.81
C16	−5486 (9)	2944 (6)	−3089 (4)	6.06
C17	−6234 (7)	1897 (5)	−3137 (4)	4.58
C18	−754 (8)	−4505 (8)	−4202 (5)	6.87
C19	73 (8)	−5744 (7)	−4037 (5)	6.73
C20	840 (8)	−6257 (7)	−4847 (6)	7.04

(10) Dong, T.-Y.; Hendrickson, D. N.; Felthouse, T. R.; Shieh, H.-S. *J. Am. Chem. Soc.* **1984**, *106*, 5373–5375.
(11) Felthouse, T. R.; Dong, T.-Y.; Hendrickson, D. N.; Shieh, H.-S.; Thompson, M. R. *J. Am. Chem. Soc.* **1986**, *108*, 8201–8214.
(12) Johnson, S. A.; Hunt, H. R.; Neuman, H. M. *Inorg. Chem.* **1963**, *2*, 960–962.

Table III, Positional Parameters ($\times 10^4$) for Compound **2**, $Rh_2(tfac)_4 \cdot NITMe$

	x	y	z	B_{eq}
Rh1	3371 (0)	7800 (0)	9044 (0)	3.13
Rh2	2537 (0)	6446 (0)	9003 (0)	3.34
O1	1859 (4)	8259 (3)	9257 (4)	4.65
O2	3813 (4)	7667 (3)	10453 (3)	3.99
O3	4847 (4)	7260 (3)	8855 (4)	4.51
O4	2890 (4)	7833 (3)	7615 (3)	4.22
O5	1073 (4)	6987 (3)	9226 (4)	4.76
O6	3048 (4)	6393 (3)	10410 (3)	4.39
O7	4071 (4)	5997 (3)	8817 (4)	4.87
O8	2054 (4)	6584 (3)	7583 (3)	4.24
C1	1083 (7)	7758 (6)	9327 (6)	4.41
C2	32 (8)	8134 (7)	9637 (8)	5.87
C3	3547 (7)	7010 (5)	10807 (6)	4.20
C4	3876 (10)	6943 (7)	11869 (6)	5.75
C5	4847 (7)	6495 (5)	8768 (6)	4.49
C6	5975 (10)	6137 (8)	8589 (12)	8.17
C7	2361 (6)	7229 (5)	7224 (5)	3.98
C8	2089 (11)	7258 (8)	6169 (8)	6.47
F1	172 (5)	8153 (4)	10554 (4)	9.14
F2	−888 (5)	7692 (4)	9341 (4)	9.34
F3	−191 (5)	8860 (4)	9309 (5)	10.42
F4	4768 (6)	7303 (6)	12239 (4)	11.57
F5	3781 (9)	6265 (4)	12217 (4)	13.70
F6	3116 (9)	7342 (7)	12253 (5)	14.74
F7	6798 (6)	6598 (5)	8676 (8)	14.88
F8	5836 (7)	5748 (8)	7837 (8)	18.68
F9	6331 (8)	5587 (7)	9193 (9)	16.83
F10	1280 (6)	6797 (5)	5785 (4)	9.99
F11	1610 (11)	7952 (6)	5887 (5)	17.12
F12	2866 (6)	7211 (12)	5797 (5)	23.87
O9	870 (4)	4084 (3)	5943 (3)	4.33
O10	1688 (5)	5200 (3)	8926 (4)	4.68
N1	733 (5)	4405 (3)	6743 (4)	3.93
N2	1119 (6)	4921 (4)	8143 (4)	4.16
C9	1576 (7)	4668 (4)	7411 (6)	4.07
C10	−409 (7)	4621 (5)	6951 (5)	4.27
C11	−109 (7)	4711 (5)	8031 (5)	4.44
C12	−1287 (7)	3976 (6)	6574 (6)	5.61
C13	−716 (8)	5436 (6)	6433 (6)	5.71
C14	−178 (8)	3901 (6)	8558 (6)	5.85
C15	−748 (8)	5375 (6)	8458 (6)	6.15
C16	2793 (7)	4687 (5)	7344 (7)	5.44

corrected for decay, Lorentz and polarization effects but not for absorption.

Structure Solution and Refinement. Crystal structures were solved by conventional Patterson and direct methods with MULTAN[13a] which led to the location of all the non-hydrogen atoms. Structure refinements were carried out by full-matrix least-squares methods with anisotropic parameters using ORXFLS3.[13b] Then, difference Fourier maps allowed for the location of all the hydrogen atoms. These were included in the final refinement models with fixed positions and isotropic thermal parameters; the final R values are reported in Table I.

Atomic positional parameters are listed in Tables II, III, IV, and V for **1**, **2**, **3**, and **4** respectively, and selected bond lengths and angles are found in Table VI. Summary of crystal data and experimental parameters (Table SI), complete listing of bond lengths (Tables SII–V), bond angles (Tables SVI–IX), anisotropic thermal parameters (Tables SX–XIII), and observed and calculated structure factors (Tables SXIV–XVII) are deposited as Supplementary Material.

Magnetic Susceptibility Measurements. The magnetic susceptibilities of the four adducts were measured between 6 and 300 K by use of an SHE 905 superconducting SQUID magnetometer operating at a field strength of 0.5 T. The data were corrected for the magnetization of the sample holder and for the diamagnetism of the constituent atoms by use of Pascal constants.

Results

Description of the Structures. Nitronyl Nitroxide Complexes. Views of the structures of the two adducts are shown in Figures 2 (**1**) and 3 (**2**).

(13) (a) Germain, G.; Main, P.; Woolfson, M. M. *Acta Crystallogr.* **1971**, *A27*, 368–376. (b) Busing, W. R.; Martin, K. U.; Levy, H. A. Oak Ridge Laboratory Report, ORNL-59-37, 1971.

Table IV, Positional Parameters ($\times 10^4$) for Compound **3**, $Rh_2(tfac)_4 \cdot (IMMe)_2$

	x	y	z	B_{eq}
Rh	2398 (0)	2679 (0)	3380 (0)	3.52
O1	1598 (1)	2402 (1)	3177 (3)	5.00
O2	2594 (1)	1911 (1)	3968 (2)	4.51
O3	3213 (1)	2930 (1)	3454 (3)	4.74
O4	2219 (1)	3424 (1)	2667 (3)	4.77
C1	1484 (2)	2164 (2)	2339 (4)	4.32
C2	888 (2)	1925 (2)	2266 (6)	5.91
C3	2736 (2)	1542 (2)	3287 (5)	4.44
C4	2849 (2)	961 (2)	3772 (6)	5.87
F1	849 (1)	1481 (1)	2805 (4)	12.66
F2	528 (1)	2263 (2)	2626 (4)	12.86
F3	739 (1)	1801 (2)	1333 (4)	13.12
F4	3311 (1)	755 (1)	3414 (4)	11.33
F5	2921 (2)	971 (1)	4775 (3)	12.41
F6	2467 (2)	619 (1)	3570 (5)	14.14
O5	2615 (1)	3259 (1)	7583 (3)	6.46
N1	2223 (1)	2997 (1)	5012 (3)	4.12
N2	2366 (2)	3238 (1)	6702 (3)	5.10
C5	2560 (2)	2961 (2)	5802 (4)	4.37
C6	3113 (2)	2668 (2)	5847 (4)	5.41
C7	1689 (2)	3268 (2)	5406 (4)	5.21
C8	1875 (2)	3591 (2)	6411 (4)	5.16
C9	1418 (2)	3615 (2)	4570 (4)	7.28
C10	1300 (2)	2771 (2)	5680 (5)	7.13
C11	1465 (2)	3631 (2)	7313 (5)	7.11
C12	2107 (2)	4177 (2)	6155 (5)	7.08

Table V, Positional Parameters ($\times 10^4$) for Compound **4**, $Rh_2(tfac)_4 \cdot IMMe$

	x	y	z	B_{eq}
Rh1	9199 (0)	6145 (0)	3033 (0)	3.50
Rh2	8948 (0)	7333 (0)	2378 (0)	3.42
O1	7997 (6)	5655 (2)	2118 (3)	4.99
O2	10394 (5)	6694 (3)	3919 (2)	4.63
O3	11181 (5)	5956 (2)	2572 (2)	4.66
O4	7188 (5)	6395 (2)	3442 (2)	4.58
O5	6928 (5)	7498 (2)	2807 (2)	4.53
O6	10100 (5)	7814 (2)	3321 (2)	4.75
O7	10979 (5)	7090 (2)	1983 (2)	4.71
O8	7823 (6)	6754 (3)	1483 (2)	4.97
C1	7644 (9)	6054 (5)	1552 (4)	4.71
C2	6965 (15)	5646 (6)	852 (5)	7.03
C3	10524 (9)	7386 (5)	3874 (4)	4.78
C4	11250 (14)	7795 (6)	4577 (5)	6.73
C5	11581 (9)	6455 (4)	2147 (4)	4.42
C6	12969 (11)	6239 (5)	1742 (5)	6.21
C7	6568 (8)	7010 (4)	3255 (4)	3.94
C8	5168 (10)	7250 (6)	3639 (5)	5.78
F1C2	5942 (9)	6044 (4)	428 (3)	13.71
F2C2	6159 (9)	5062 (4)	959 (3)	13.85
F3C2	7947 (8)	5437 (5)	471 (4)	18.47
F1C4	12208 (8)	7372 (4)	4999 (3)	13.16
F2C4	10240 (7)	7988 (5)	4966 (3)	15.47
F3C4	12039 (9)	8376 (4)	4464 (3)	13.79
F1C6	14113 (5)	5939 (3)	2203 (3)	9.29
F2C6	13577 (6)	6828 (3)	1472 (3)	11.17
F3C6	12558 (7)	5780 (4)	1224 (3)	12.92
F1C8	4565 (7)	6688 (3)	3953 (4)	12.69
F2C8	4084 (6)	7560 (4)	3221 (3)	13.54
F3C8	5628 (6)	7695 (4)	4178 (3)	12.65
O9	10495 (6)	10045 (2)	1272 (2)	5.33
N1	8816 (7)	8431 (3)	1831 (3)	4.26
N2	9556 (7)	9520 (3)	1387 (3)	4.31
C9	9972 (9)	8889 (4)	1812 (4)	4.52
C10	11630 (8)	8832 (4)	2175 (4)	5.96
C11	7953 (9)	9403 (4)	943 (4)	4.53
C12	7333 (9)	8821 (4)	1460 (4)	4.57
C13	7070 (9)	10144 (4)	824 (4)	6.13
C14	8224 (11)	9082 (5)	201 (4)	7.37
C15	6161 (9)	8275 (4)	1050 (4)	5.77
C16	6615 (9)	9208 (4)	2101 (4)	6.22

One formula unit of **1** comprises the unit cell with crystallographic centers of inversion located at the midpoint of the Rh–Rh

Table VI. Selected Bond Lengths (Å) and Angles (deg)

	(a) $Rh_2(tfac)_4(NITPh)_2$, **1**		
Rh–Rh	2.412 (1)	O1–Rh–O2 (av)	89.9 (3)
Rh–O1	2.034 (3)	Rh–Rh–O9	174.9 (1)
Rh–O9	2.239 (3)	Rh–O9–N1	122.7 (3)
N1–O9	1.309 (4)		
N2–O10	1.268 (5)		
	(b) $Rh_2(tfac)_4$ NITMe, **2**		
Rh1–Rh2	2.407 (1)	O1–Rh–O2 (av)	89.9 (1)
Rh–O1 (av)	2.026 (5)	Rh2–Rh1–O9	178.8 (1)
Rh1–O9	2.268 (5)	Rh1–Rh2–O11	177.6 (2)
Rh2–O11	2.254 (5)	Rh1–O9–N1	118.3 (4)
N1–O9	1.301 (7)	Rh2–O11–N2	121.3 (4)
N2–O11	1.290 (7)		
	(c) $Rh_2(tfac)_4$ $(IMMe)_2$, **3**		
Rh–Rh	2.4323 (8)	O1–Rh–O2 (av)	89.5 (1)
Rh–O1 (av)	2.035 (3)	Rh–Rh–N1	178.9 (1)
Rh–N1	2.237 (4)		
N2–O9	1.262 (5)		
	(d) $Rh_2(tfac)_4$ IMMe, **4**		
Rh1–Rh2	2.4191 (8)	O1–Rh–O2 (av)	90.3 (2)
Rh–O1 (av)	2.032 (2)	Rh2–Rh1–N1	176.9 (2)
Rh1–N1	2.188 (5)	Rh1–Rh2–O9	176.5 (1)
Rh2–O9	2.320 (5)	Rh1–O9–N2	123.6 (4)
N2–O9	1.274 (6)		

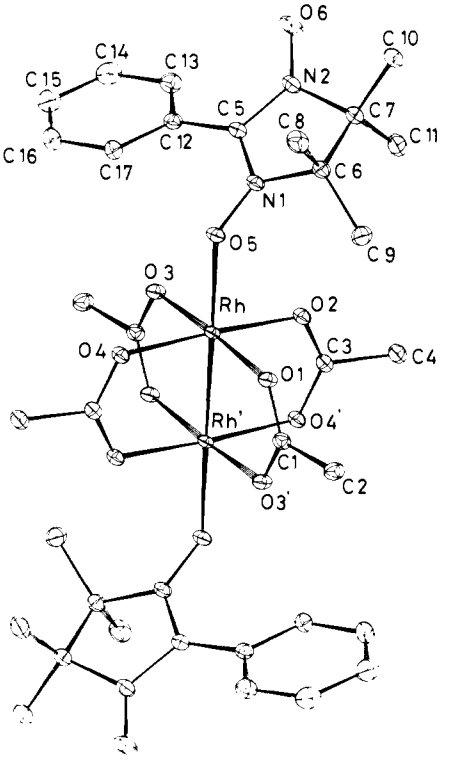

Figure 2. Molecular structure of compound **1**, $Rh_2(tfac)_4$·$(NITPh)_2$, showing 30% probability ellipsoids and the atom numbering scheme.

bond and the center of the benzene solvate molecule. The central $Rh_2(O_2C_2)_4$ core displays essentially D_{4h} symmetry. Each Rh atom is in a tetragonally elongated environment, one of the axial positions being occupied by a nitroxyl oxygen atom at a bonding distance of 2.239 (3) Å. The Rh–Rh bond length is 2.412 (1) Å in accord with previous structures of this type.[11,14] The distribution of the C–F distances (1.245–1.322 Å) and the C–C–F angles (110–115°) arises from the highly anisotropic motion of the fluorine atoms.

(14) Felthouse, T. R. *Prog. Inorg. Chem.* **1982**, *29*, 73–166.

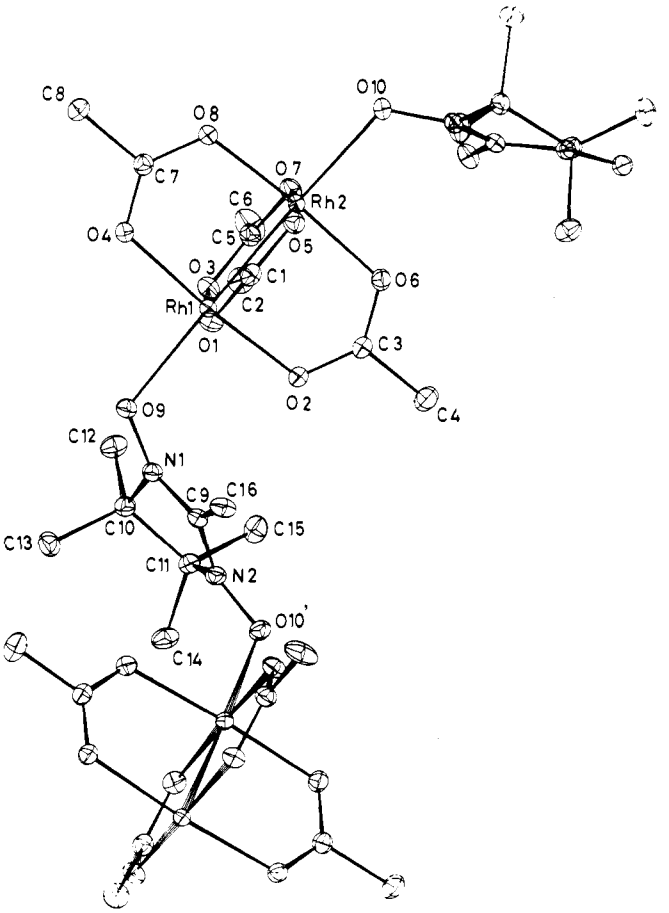

Figure 3. Molecular structure of compound **2**, $Rh_2(tfac)_4$·NITMe, showing 30% probability ellipsoids and the atom numbering scheme.

The NITPh ligands have the usual shape[15-17] with a planar O5–N1–C5–N2–O6 fragment, and a five-membered ring twisted out as a result of the probably preferred staggered conformation of the methyl groups. The 2-phenyl ring makes an angle of 37° with the planar π-system of the heterocycle. Close inspection of Table VI shows that the N1–O5 bond length involving the coordinated oxygen atom, is significantly longer, by 0.041 (9) Å, than the N2O6 distance. Some intermolecular contacts involve the uncoordinated NO groups of the NITPh ligands which are arranged head to tail at the corners of a parallelogram. Therefore, the structure of **1** can be described as chains along the *c* axis. Since they are of importance in determining the magnitude of the magnetic interactions, these intermolecular contacts are extensively described in the discussion for the four compounds.

On the other hand, the NITMe adduct **2**, is an extended linear chain of alternating dirhodium carboxylates and nitroxyl free radicals, elongated along the *b* axis (Figure 3). The dirhodium core is almost identical with that found in compound **1**; however, there is no center of inversion at the midpoint of the Rh–Rh bond, and slightly different Rh–O(nitroxyl) bond lengths (2.268 (5) and 2.254 (5) Å) are observed. For the same reason the Rh–Rh–O (nitroxyl) angles (178.8 (1) and 177.6 (2)°) also are different but close to 180°.

Ignoring the nature of the substituent in position 2 of the nitroxide, the NITMe and NITPh fragments have the same structural characteristics. However, in **2**, the NITMe ligand bridges two rhodium dimers and since in that case the two NO groups are metal-bound, the NO bond lengths are of the same order of magnitude (1.301 (7) and 1.290 (7) Å) and larger than

(15) Wong, W.; Watkins, S. F. *J. Chem. Soc., Chem. Commun.* **1973**, 888–889.
(16) Laugier, J.; Rey, P.; Benelli, C.; Gatteschi, D.; Zanchini, C. *J. Am. Chem. Soc.* **1986**, *108*, 6931–6937.
(17) Gatteschi, D.; Laugier, J.; Rey, P.; Zanchini, C. *Inorg. Chem.* **1987**, *26*, 938–943.

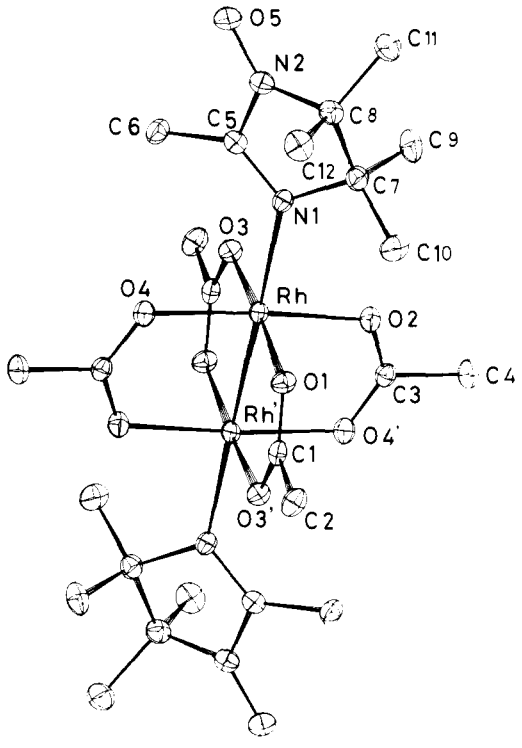

Figure 4. Molecular structure of compound 3, $Rh_2(tfac)_4 \cdot (IMMe)_2$, showing 30% probability ellipsoids and the atom numbering scheme.

the uncoordinated one (1.268 (4) Å) in NITPh.

For both compounds the Rh–O–N angles (122.7 (3)° in **1**, 118.3 (4)° and 121.3 (4)° in **2**) are within a few degrees from 120°.

Imino Nitroxide Adducts. Compound **3**, as shown in Figure 4, is a bis-nitroxyl adduct in which only the imino nitrogen atoms of the two imino nitroxide ligands are coordinated. As for compound **1**, a center of inversion is located at the midpoint of the Rh–Rh bond, the length of which is 2.4323 (8) Å. Each rhodium atom is in a distorted octahedral environment, the exogenous axial position being occupied by the imino atom of the ligand at a bonding distance of 2.337 (4) Å, longer than that found for the Rh–O bond in the analogous O-bonded nitronyl complex **1**.

Although the study of this adduct affords the first structural determination of an imino nitroxide, the characteristics of the free-radical moiety are close to those observed for the nitronyl analogues and need only a few comments. The conjugated imino-nitroxyl fragment is planar but no longer symmetrical; the imino nitrogen atom is now short bonded to the adjacent carbon indicating a more localized electronic structure. This is in agreement with the solution EPR spectra which show different coupling constants for the two nitrogen atoms.[7] A NO bond length of 1.262 (5) Å is observed, equal to the corresponding one in compound **1**, and it can be inferred that this bond length has the same value in the isolated nitroxide as well. Noteworthy is the fairly close orthogonality (97.7°) of the plane of the nitroxyl π-system with the basal plane of the rhodium atoms.

In the fourth complex, shown in Figure 5, the imino nitroxide ligand bridges two $Rh_2(tfac)_4$ moieties leading to a chain of alternating rhodium dimers and free radicals extended along the *c* axis. The metal dimer fragment is very similar to those observed in the other three adducts, with a Rh–Rh bond length of 2.4191 (8) Å. The exogenous apical positions of the two rhodium atoms are occupied, respectively, by an oxygen and a nitrogen atom belonging to two different nitroxides at bonding distances of 2.320 (5) and 2.188 (5) Å, respectively. Among the series, this compound has the largest Rh–O and the shortest Rh–N bond lengths; the Rh–Rh–O and the Rh–Rh–N angles are close to 180° (176.5 (1) and 176.9 (2)°).

The nitroxide fragment is identical with that described in complex **3**, with a π-plane perpendicular (88.6°) to the basal plane of the rhodium atom bound to the imino nitrogen. This π-plane

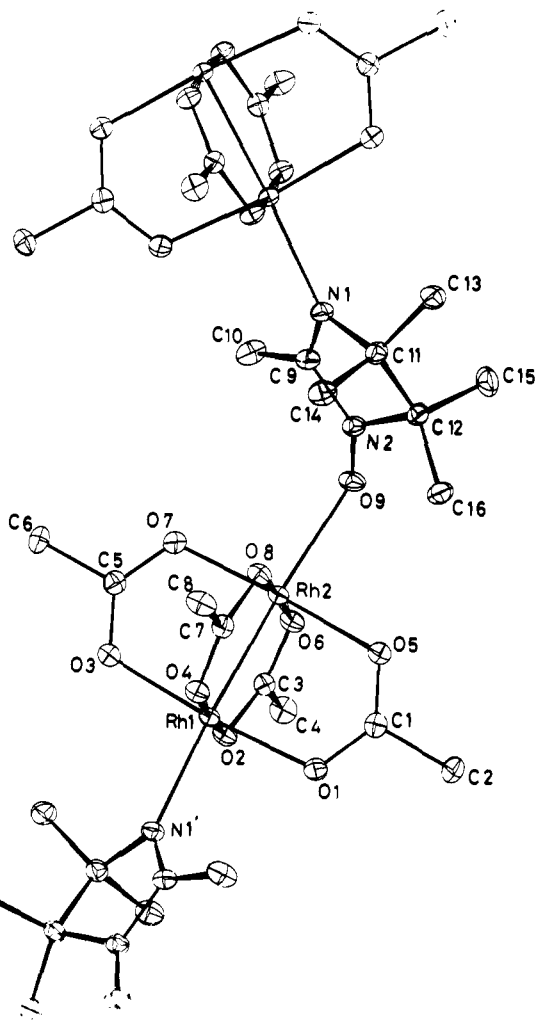

Figure 5. Molecular structure of compound 4, $Rh_2(tfac)_4 \cdot IMMe$, showing 30% probability ellipsoids and the atom numbering scheme.

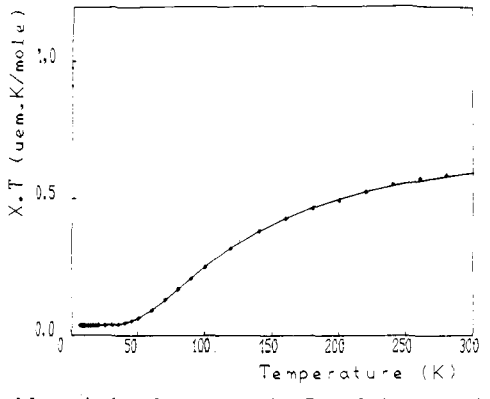

Figure 6. Magnetic data for compound 1, $Rh_2(tfac)_4 \cdot (NITPh)_2$, in the form of XT vs T. The solid line is calculated with the parameters reported in Table VII.

makes an angle of 43.4° with the basal plane of the O-bonded metal atom, the Rh–O–N angle being 123.6 (4)°.

Magnetic Properties. Magnetic data are found in Figures 6–9 for compounds **1**–**4**, respectively, in the form of XT vs T. In addition is reported, in Figure 7, the temperature dependence of the magnetic susceptibility of **2**, which shows the typical behavior of a linear chain of antiferromagnetically coupled spins $S = 1/2$. Qualitative features may also be noticed for the other adducts: as shown in Figures 6 and 8 the decrease of the XT value with decreasing temperature is that expected for antiferromagnetically coupled species, while the increase observed for **4** (Figure 9) may be accounted for by ferromagnetic interactions.

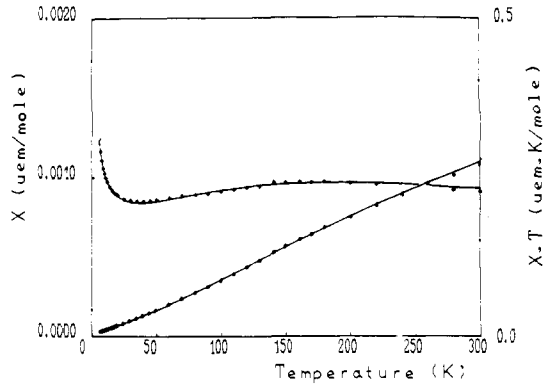

Figure 7. Magnetic data for compound **2**, $Rh_2(tfac)_4$,NITMe, in the form of X and XT vs T. The solid line is calculated with the parameters reported in Table VII.

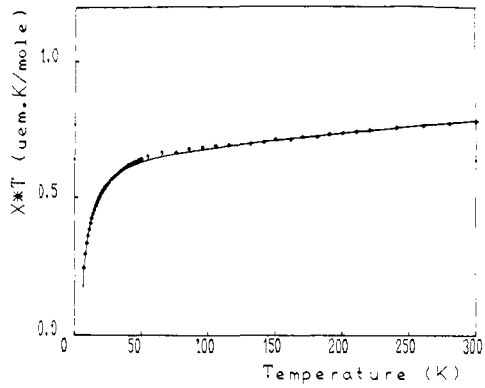

Figure 8. Magnetic data for compound **3**, $Rh_2(tfac)_4$,$(IMMe)_2$, in the form of XT vs T. The solid line is calculated with the parameters reported in Table VII.

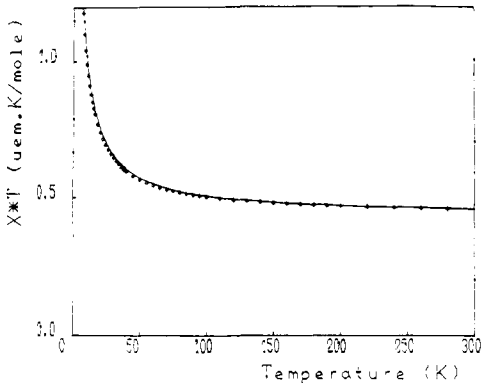

Figure 9. Magnetic data for compound **4**, $Rh_2(tfac)_4$,IMMe, in the form of XT vs T. The solid line is calculated with the parameters reported in Table VII.

The X-ray results afford models for interpreting these data. Thus, the magnetic data of the two bis-adducts **1** and **3** were fit to a Bleaney–Bowers equation[18] of the form

$$X_m = (Ng^2\mu^2/kT)(2/(3 + \exp(-2J/kT)))$$

Owing to the chain structure observed for **2** and **4**, chain models were attempted. As noticed before, compound **2** exhibits an antiferromagnetic behavior, while for **4**, the increase of XT at low temperature is indicative of predominant ferromagnetic interactions. Although these chain models cannot be solved exactly at present, numerical data for the generation of the magnetic susceptibilities have been developed in both cases. Accordingly, the magnetic data of **2** were fit to the following expression[19,20]

$$X_m = (Ng^2\mu^2/kT)(0.25 + Bx + Cx^2)(1 + Dx + Ex^2 + Fx^3)^{-1}$$

(18) Bleaney, B.; Bowers, K. D. *Proc. Roy. Soc.* **1952**, *A214*, 451–465.

Table VII. Fitting Parameters of the Magnetic Data

compd	$2J$ (cm^{-1})	g	a (%)	TIP(10^6)	$F(10^4)^a$
$Rh_2(tfac)_4$,$(NITPh)_2$, **1**	−167.2	1.998	0.9	142	6
$Rh_2(tfac)_4$,NITMe, **2**	−197.6	2.114	0.3	126	1.5
$Rh_2(tfac)_4$,$(IMMe)_2$, **3**	−10.4	1.976	0.2	49	3.8
$Rh_2(tfac)_4$,IMMe, **4**	+4.6	2.122	1.3	10	1.6

[a] The function minimized in the fitting process was $F = \sum(X^{obsd} - X^{calcd})^2/\sum(X^{obsd})^2$.

where $x = -J/kT$, and constants B–F are power series in term of α of the alternation parameter. It is worth noting that, in the present case, $\alpha = 1$ since the crystal structure does not require an alternating model. This parameter was thus held constant in the fitting process; however, we have checked that no better fit could be obtained by varying its value.

The equation used in the fitting process of the magnetic data of complex **4** has the following form[21]

$$X_m = (Ng^2\mu^2/4kT)((1 + 5.8K + 16.9K^2 + 29.38K^3 + 29.83K^4 + 10.04K^5)/(1 + 2.8K + 7.01K^2 + 8.65K^3 + 4.57K^4))^{2/3}$$

where $K = J/2kT$.

In all the samples of **1** that we have studied, there was evidence of a paramagnetic impurity as revealed by the increase of the X value below 30 K. Accordingly, the expressions to which the magnetic data were fit were modified. The magnetic behavior of the impurity was assumed to follow a Curie law with a g value of 2.0 since it is necessarily the uncoordinated nitroxide. The parameters best fitting our data to these modified expressions are reported in Table VII. It can be noticed that the two O-bonded adducts exhibit fairly strong internitroxyl antiferromagnetic interactions, while the N-bonded ones display weak couplings. The g values (1.976–2.114) as well as the TIP values (10–140 10^{-6}) are less accurately determined because these are essentially independent of the temperature behavior of the magnetism; weighing and calibration errors and the presence of diamagnetic impurities would all show up as an effect on these parameters.

Discussion

We recently reported the syntheses of the adducts of NITPh with copper(II) chloride[16] and copper(II) bis(hexafluoroacetylacetonate).[17] In both adducts the nitroxide is metal-oxygen bound only by one of its two NO sites. This bonding pattern, which is also observed in the present investigation, seems to be usual with this ligand and must be related to the steric hindrance of the phenyl group. As mentioned before, the O–N–C–N–O fragment is planar, and the crowding of the two potentially coordinating oxygen atoms by the phenyl ortho-hydrogen atoms is identical. In addition each site is hindered by one *gem*-dimethyl at distances of 2.8–3.0 Å. The same situation is observed in NITMe concerning the methyl groups, but, in this case, the smaller methyl substituent in position 2 leads to a better coordinating ability of the NO groups. Thus, in the potentially bidentate nitroxide, NITPh, only one site of coordination is active, and compound **1** is a bis-nitroxyl complex as observed for the adducts with $CuCl_2$ and $Cu(hfac)_2$; this adduct is similar to those recently described by Hendrickson et al. for the monodentate nitroxide Tempo.[11] On the other hand, in NITMe the smaller methyl group allows for the coordination of both NO groups to metal atoms, and compound **2** is a chain of nitroxide free radicals bridged by rhodium carboxylate dimers.

Surprising is the preferred N-coordination of the imino nitroxide in complex **3**, because the imino nitrogen is expected, at first sight, to be less accessible to metal ions than the oxygen atom. Shorter *gem*-dimethyl nitrogen distances are indeed observed (2.4–2.6 Å); we believe therefore, that it is the more pronounced basic character of the imino group which is responsible for the preferred nitrogen

(19) Duffy, W.; Barr, K. P. *Phys. Rev.* **1968**, *165*, A647–A654.
(20) Hall, J. W.; Marsh, W. E.; Weller, R. R.; Hatfield, W. E. *Inorg. Chem.* **1981**, *20*, 1033–1037.
(21) Baker, G. A., Jr.; Rushbrooke, G. S.; Gilbert, H. E. *Phys. Rev.* **1964**, *135*, A1272–A1277.

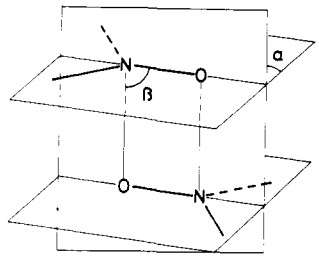

Figure 10. Definition of the structural parameters reported in Table IX for the description of the intermolecular interactions.

ligation in **3**. However, this preference does not hamper the coordination at the NO site which is metal bound in **4**. It is worth noting that the obtention of the latter is determined only by the proportion of the reactants.

Among the series, one observes O-bonded complexes exhibiting fairly large antiferromagnetic interactions and N-bonded adducts which display weak (positive or negative) internitroxyl couplings. Three reasons can be invoked for such a difference: (i) the nitronyl and the imino nitroxides have different electronic structures, (ii) the observed magnetic data are the consequence of *intermolecular* rather than *intramolecular* interactions, and (iii) the bonding geometry of the free radicals to the dirhodium fragment is responsible for the large difference in the internitroxyl couplings. Our discussion will consider successively these three points.

Electronic Structure of the Nitronyl and Imino Nitroxides. Copper(II) adducts of some nitronyl nitroxides[8,17,22] display the same magneto-structural correlations as those observed for the Tempo derivatives (vide infra), and recent theoretical calculations[22] have shown that the electronic structure of the former closely resembles that of Tempo. On the other hand, no metal adduct or theoretical treatments of the imino nitroxides have been reported yet. Since the magnetic properties of our complexes may depend to a large extent on the electronic structure of the nitroxide ligands, we performed extended Hückel[23] calculations to get a semiquantitative insight into the SOMO's of the nitronyl and imino nitroxides. In both cases the unpaired electron is found, as expected,[24] in a MO of π^* symmetry involving almost exclusively the 2pz (z refers to the axis perpendicular to the N–C–N plane) orbitals of the O–N–C–N–O and the N–C–N–O atoms for NITMe and IMMe, respectively. In Table VIII are reported the estimated spin populations located on these atoms in both cases; for comparison the result of the same calculations for Tempo is included. It is worth noting that the imino nitrogen atom in IMMe bears more spin density than either oxygen atom in NITMe. However, owing to the delocalization of the unpaired electron the spin population on the oxygen atoms in NITMe and IMMe is roughly half that found in Tempo. It is therefore clear that the small coupling observed for the N-bonded adducts is not the consequence of a very low spin population on the bound imino nitrogen atom. On the other hand, it can be already inferred that the larger spin population found on the Tempo oxygen atom is one of the determining factors for the large internitroxyl coupling reported for the dirhodium Tempo derivatives,[11] **6** and **7** (Figure 1).

Intermolecular Interactions. The interpretation of the magnetic data is supported by the structural results ignoring any intermolecular interaction. Despite the reasonable agreement obtained by using these models, one can note that the data concerning the bis-adducts **1** and **3**, could have been interpreted with the same pair model but considering only intermolecular through-space couplings between uncoordinated NO groups. Therefore we have to examine if the reported $2J$ values may be the consequence of some intermolecular short contacts. Recently, Hendrickson et al.[11] have reported a compilation of relevant examples which provide a statistical basis for comparisons with the magnetic data for **6** and **7**. By using slightly different structural parameters defined in Figure 10, we have built Table IX which lists the shortest intermolecular contacts in compounds **1–4**. Compound **5** (Figure 1) is the only metal derivative of a nitronyl nitroxide in which the magnitude of a nitroxyl–nitroxyl *intermolecular* interaction has been accurately determined;[6] it has, therefore, been included in the table for comparison. In the five compounds the nitroxyl–nitroxyl group contacting occurs with head-to-tail alignment of the NO bonds at the corners of a parallelogram. The spatial overlap of the π^* orbitals, at a given O–N′ distance, will be maximum for $\alpha = \beta = 90°$. It can be seen from Table IX that the orientation of the NO groups in **5** approaches this optimum for formation of a through-space interacting radical pair. Since in this compound the singlet–triplet splitting is only of -15 cm^{-1}, no larger interactions are expected for compounds **1–4**, in which the O–N′ distances are larger and the α and β angles are farther from the 90° optimum value. This analysis provides compelling evidence that the fairly large antiferromagnetic spin coupling in the O-bonded adducts, **1** and **2**, arises mainly from an *intramolecular* through-bond interaction involving the $Rh_2(O_2CF_3)_4$ core, as reported for the Tempo adducts, **6** and **7**.[11] The magnetic behavior of the two N-bonded adducts, **3** and **4**, in which the couplings are so small, provides further evidence that through-space interactions are insignificant in **1** and **2**. On the contrary, for these N-bonded complexes, we have to consider both inter- and intramolecular interactions.

More importantly we have to explain these unexpectedly weak exchange couplings in the two imino nitroxide derivatives compared to the nitronyl nitroxide analogues. Since it is established that the magnitude of the internitroxyl interaction in the latter is mediated by the dirhodium fragment, the origin of this difference must be reflected in the structural characteristics of the rhodium–nitroxyl bonding in each class of complexes.

Bonding Geometry of the Nitroxyl Group and Magnetic Properties. Relevant examples of metal–nitroxide bonding geometries are found in copper derivatives. They can be grouped into two classes, each possessing characteristic structural and magnetic features. Schematically, complexes with short-bonded equatorial nitroxyl ligands exhibit strong antiferromagnetism,[16,25-28] while

Table VIII. Distribution of the Spin Population in the Nitronyl and Imino Nitroxides

compd	O	N1	C	N2	O
NITMe	0.15	0.31	0.0	0.31	0.15
IMMe	0.23	0.32	0.04	0.28	
Tempo	0.31	0.57			

Table IX. Closest Intermolecular Contacts

compd	d (Å)	α^a (deg)	β^a (deg)	$2J$ (cm^{-1})
$Rh_2(tfac)_4$·$(NITPh)_2$, **1**	4.11	61.2	108.2	−167.2
$Rh_2(tfac)_4$·NITMe, **2**	4.69	51.9	99.2	−197.6
$Rh_2(tfac)_4$·$(IMMe)_2$, **3**	3.68	63.1	100.6	−10.4
$Rh_2(tfac)_4$·IMMe, **4**	4.88	54.5	96.4	+4.6
$CuCl_2$·$(NITPh)_2$, **5**	3.59	75.3	93.6	−15.2

[a] For the definition of α and β see Figure 10.

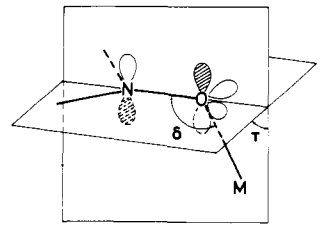

Figure 11. Electronic structure of the nitroxyl group and description of the angular bonding parameters.

(22) Caneschi, A.; Gatteschi, D.; Grand, A.; Laugier, J.; Pardi, L.; Rey, P. *Inorg. Chem.* **1988**, *27*, 2027–2032.
(23) Tolpin, E. I. *QCPE* **1978**, *10*, 358.
(24) Morishima, I.; Yoshikawa, K.; Yonezawa, T. *Chem. Phys. Lett.* **1972**, *16*, 336–339.
(25) Lim, Y. Y.; Drago, R. S. *Inorg. Chem.* **1972**, *11*, 1334–1338.
(26) Dickman, M. H.; Doedens, R. J. *Inorg. Chem.* **1981**, *20*, 2677–2681.
(27) Porter, L. C.; Doedens, R. J. *Inorg. Chem.* **1985**, *24*, 1006–1010.

Table X. Bonding Parameters for the Rhodium–Nitroxyl Complexes

compd	d (Å)	δ^c (deg)	τ^c (deg)	sin δ sin τ
$Rh_2(tfac)_4$·(NITPh)$_2$, **1**	2.239	122.7	89.5	0.84
	2.268	118.3	65.3	0.84
$Rh_2(tfac)_4$·NITMe, **2**	2.254	121.3	107.2	0.78
$Rh_2(tfac)_4$·(IMMe)$_2$, **3**	2.237			0.19[a]
	2.188			0.03[a]
$Rh_2(tfac)_4$·IMMe, **4**	2.330	123.6	95.8	0.82
$Rh_2(tfac)_4$·(Tempo)$_2$, **6**[b]	2.220	138.0	88.1	0.67
$Rh_2(hfbu)_4$·(Tempo)$_2$, **7**[b]	2.235	134.2	83.8	0.71

[a] For the N-bonded rhodium sites are reported the sin of the angle between the $Rh-O_4$ plane and the C–N–C plane. These values are proportional to the σ component of the nitroxyl π^* orbital. [b] See ref 11. [c] For the definition of δ and τ see Figure 11.

those containing a long bonded axial nitroxide exhibit a ferromagnetic behavior.[4,5,8,17,22,29,30] Bonding of the nitroxide in these complexes is believed to occur through one of the two lone pairs of the sp^2 hybridized oxygen atom, in a σ fashion. However, careful examination of the structural parameters does not allow us to draw such a straightforward picture. In Figure 11 is depicted the electronic structure of the nitroxyl group. The unpaired electron resides in an orbital of π^* symmetry, orthogonal to the C–N–C plane, while the two oxygen lone pairs lay in the C–N–C plane. In the first class of antiferromagnetic complexes, the Cu–O–N angle (δ) is generally close to 120°, whereas the N–O–Cu plane is found to be perpendicular to the C–N–C plane (τ = 90°). This last result is strongly at variance with the above lone pair bonding description. In the second class of compounds, the Cu–O–N angle is close to 180°, the discrepancy being more pronounced. Therefore, this simple description, using localized lone pairs must be revised. More than 10 years ago, was reported a theoretical treatment of the reactivity in nitroxides through ab initio molecular electrostatic potential,[31] which affords a more comprehensive picture of the bonding geometry of the nitroxides. Although the expected lone pair directions are the more probable for bonding interactions, the potential curves show a wide attractive region surrounding the oxygen atom. In this description, all the directions such that the M–O–N angle is 120° are nearly equivalent. Further support to this result comes from the early work of Hoffmann et al.[32] on the nitroxyl complexes of the IIIA group halides. In these adducts with diamagnetic Lewis acids, it was shown by EPR that the ligation of the nitroxyl oxygen atom occurs with displacement of the unpaired spin density toward the nitrogen atom. In other words, the description of the nitroxide group, once bound, must include in part the characteristics of the ionic limit formula in which the oxygen atom is negatively charged and has six nonbonding electrons and a nearly isotropic surrounding. It is therefore likely that the electronic factors do not play the main role in determining the bonding geometry in copper–nitroxyl complexes, these actual geometries being better explained by steric crowding considerations. Indeed, the close orthogonality of the C–N–C and the M–O–N planes (τ) places the metal atom in the space region which is not crowded by the nitroxyl methyl groups. It is worth noting also that, at a given Cu–O distance, this arrangement provides the largest overlap between the nitroxyl π^* orbital and the metal orbital pointing toward the oxygen. This explains the observed antiferromagnetism in the first class of complexes. It is very likely that the bonding geometry of the axially bound complexes also is determined by steric crowding; these complexes have Cu–O–N angles close to 180°, and they exhibit weak ferromagnetic couplings as a consequence of the orthogonality[33] of the nitroxyl π^* and copper $d_{x^2-y^2}$ orbitals. Similar magneto-structural correlations are observed in the few reported copper(II) nitronyl nitroxide derivatives.[8,16,17]

Table X assembles pertinent structural bonding parameters in compounds **1**–**7**. Our rhodium dimer adducts all show large metal–nitroxyl distances but dramatic differences in their angular bonding parameters and magnetic properties. The O-bonded derivatives **1** and **2** (as well as the Tempo adducts **6** and **7**) are closely related to the antiferromagnetic copper complexes with δ and τ angle values close to 120° and 90°, respectively, while the N-bonded adducts **3** and **4** exhibit the typical coordination pattern of the weakly coupled copper nitroxyl adducts with a C–N–C plane approximately perpendicular to the basal plane of the metal atom. However, because in our series the nitroxyl π^* orbitals do not interact directly and must rely on spin density over the dirhodium fragment, this analogy with the copper complexes does not explain the magnetic data; but it is clear that the overlap between the appropriate orbital of the dirhodium fragment and the π^* orbital of the nitroxides obeys a similar angular dependence.

The most commonly accepted description of the energy level ordering of the dirhodium fragment is provided by the SCF-Xα-SW calculation of Norman and Kolari.[34] Within the $\pi^4\ \sigma^2\ \delta^2\ \pi^{*4}\ \delta^{*2}$ manifold, interaction of the π^* nitroxyl orbital with the δ orbitals is symmetry forbidden, and only π or σ interactions are allowed. To relate the structural parameters of the bonding between the Rh_2 core and the axial ligands, it is convenient to divide each nitroxide (O- or N-bonded) SOMO into a σ component collinear with the Rh–Rh bond and a π component parallel to the $Rh-O_4$ plane. In the O-bonded adducts with Rh–O–N angles close to 120°, the nitroxide σ and π components are nearly equivalent. Therefore, depending on the Rh–Rh energy level ordering, both Rhσ–NOσ and Rhπ–NOπ overlap can be involved in the internitroxyl magnetic coupling. In the previously reported centrosymmetric adducts **6** and **7**, the large antiferromagnetic interaction has been accounted for by Rhπ^*–NOπ^* back bonding. Although this mechanism is in agreement with the properties of compound **1**, the other adducts afford new geometrical schemes. The extended linear O-bonded compound **2** deserves special mention since the two nitroxide π components are no longer parallel, as found in the centrosymmetric adducts, but orthogonal (91.2°).[1] Owing to this orthogonality, a Rhπ–NOπ overlap cannot be responsible for the coupling of the nitroxyl ligands. On the contrary, there is no symmetry limitation for the interaction of a Rh σ orbital with the two σ components of the nitroxyl groups, and we suggest that, in all cases studied so far, it is this mechanism which is responsible for the magnitude of the observed couplings. Bearing in mind that the electronic structures of the nitronyl and imino nitroxides are closely related, further strong support for this σ mechanism comes from the magnetic behavior of the two remaining N-bonded complexes. In these adducts, containing one or two axially bound nitrogen atoms, owing to the near orthogonality of the nitroxide least-squares plane and the $Rh-O_4$ plane, the large nitroxide π components would give a large interaction if the symmetry-allowed interacting orbital on the Rh–Rh fragment was of π symmetry. On the other hand if the interacting orbital is of the σ type, the overlap is symmetry forbidden, and the nitroxyl–nitroxyl coupling is expected to be weak (positive or negative) as observed. Thus, these local symmetry considerations clearly show that the magnetic behavior of complexes **1**–**4**, **6**, and **7** is better explained by a nitroxyl–nitroxyl coupling mechanism involving a Rh–Rh orbital of σ symmetry.

As the data in Table X show, an estimate of the σ component of the nitroxyl π^* orbital in each complex can be obtained from the angular bonding parameters. Assuming that the Rh, Rh, and O atoms are collinear, this σ component is proportional to sin δ sin τ. If the Rh–O (or N) distances and the structures of the dirhodium cores were identical in all the compounds among the series, the overlap between the magnetic orbitals would also be proportional to the values of this product. Although this is not the case, it can be noticed that the magnitude of the $2J$ values

(28) Porter, L. C.; Dickman, M. H.; Doedens, R. J. *Inorg. Chem.* **1986**, *25*, 678–684.
(29) Grand, A.; Rey, P.; Subra, R. *Inorg. Chem.* **1983**, *22*, 391–394.
(30) Benelli, C.; Gatteschi, D.; Zanchini, C.; Latour, J.-M.; Rey, P. *Inorg. Chem.* **1986**, *26*, 4242–4244.
(31) Ellinger, Y.; Subra, R.; Berthier, G.; Tomasi, J. *J. Phys. Chem.* **1975**, *79*, 2440–2443.
(32) Eames, T. B.; Hoffman, B. M. *J. Am. Chem. Soc.* **1971**, *93*, 3141–3146.
(33) Kahn, O.; Charlot, M.-F. *Nouv. J. Chim.* **1980**, *4*, 567–576.
(34) Norman, J. G., Jr.; Kolari, H. J. *J. Am. Chem. Soc.* **1978**, *100*, 791–799.

follows the same trend as those of the σ components. However this simple description does not explain the magnitude of the couplings in the Tempo adducts, **6** and **7**, compared to those observed in the nitronyl analogues. Fortunately, however, in compounds **1** and **7**, the Rh-O(nitroxyl) distances and the structural characteristics of the dirhodium fragments are almost identical; thus a quantitative comparison was attempted.

The magnetic orbitals are defined as singly occupied orbitals centered on the nitroxyl groups, A and B, respectively, and partially delocalized on the dirhodium fragment. Taking into account that the two compounds are centrosymmetric, these orbitals may be written at the first order of perturbation theory as

$$\Phi A = a\mathrm{Rh}(\sigma) + \mathrm{NOA}(\pi^*)$$

$$\Phi B = a\mathrm{Rh}(\sigma) + \mathrm{NOB}(\pi^*)$$

where $a = \langle \mathrm{NO}(\pi^*)||H||\mathrm{Rh}(\sigma)\rangle/\Delta$, H being the monoelectronic Hamiltonian, $\mathrm{NOA}(\pi^*)$ and $\mathrm{NOB}(\pi^*)$ the SOMO's of the two nitroxides, $\mathrm{Rh}(\sigma)$ the matching dirhodium MO, and Δ the energy gap between the NO and the Rh orbitals. The antiferromagnetic interaction is proportional to $-S^2$, with

$$S = \langle \Phi A/\Phi B\rangle = a^2\langle \mathrm{Rh}(\sigma)/\mathrm{Rh}(\sigma)\rangle + 2a\langle \mathrm{Rh}(\sigma)/\mathrm{NO}(\pi^*)\rangle + \langle \mathrm{NOA}(\pi^*)/\mathrm{NOB}(\pi^*)\rangle$$

Since the unpaired electrons are expected to be mainly localized on the nitroxides, a is small, and $a^2\langle \mathrm{Rh}(\sigma)/\mathrm{Rh}(\sigma)\rangle$ can be neglected. In addition, direct $\langle \mathrm{NO}/\mathrm{NO}\rangle$ overlap is expected to be very weak because no internitroxyl coupling would be observed if the rhodium fragment was absent; therefore, $\langle \mathrm{NO}(\pi^*)/\mathrm{NO}(\pi^*)\rangle$ can also be neglected. Thus,

$$\begin{aligned} S &\approx 2a\langle \mathrm{Rh}(\sigma)/\mathrm{NO}(\pi^*)\rangle \\ &\approx 2\langle \mathrm{Rh}(\sigma)/H/\mathrm{NO}(\pi^*)\rangle\langle \mathrm{Rh}(\sigma)/\mathrm{NO}(\pi^*)\rangle/\Delta \\ &\approx 2\langle \mathrm{Rh}(\sigma)/\mathrm{NO}(\pi^*)\rangle^2/\Delta \end{aligned}$$

The π^* nitroxyl orbitals are linear combinations of the form

$$\mathrm{NO}(\pi^*) = c2\mathrm{p(O)} + d2\mathrm{p(N)} + \ldots$$

in which only the 2p orbital of the bound oxygen atom (2p(O)) is expected to contribute significantly to the magnetic orbitals. Thus

$$S \approx 2c^2\langle \mathrm{Rh}(\sigma)/2\mathrm{p(O)}\rangle^2 = 2\rho\langle \mathrm{Rh}(\sigma)/2\mathrm{p(O)}\rangle^2$$

where ρ is the spin population on the bound oxygen atom (Table VIII). Assuming that the energy gap between the interacting orbitals is the same in compounds **1** and **7** and taking the values of the overlap integrals as $\sin\delta \sin\tau$ from Table X, one obtains

$$(S_1/S_7)^2 = \{(\rho_1/\rho_7)(\sin\delta_1 \sin\tau_1/\sin\delta_7 \sin\tau_7)\}^2$$

$$= (0.16/0.31)^2*(0.84/0.71)^2 = 0.36$$

This value is in fairly good agreement with the experimental ratio

$$J_1/J_7 = 167/538 = 0.31$$

It appears therefore, that a σ mechanism explains quantitatively the magnetic data for the two closely related complexes **1** and **7**.

Thus, an appropriate view of the bonding in these adducts implies that a σ or σ^* orbital of the metal fragment is close in energy with the π^* nitroxyl orbitals. A qualitative support to this view comes from EHT calculations performed on compound **1** and on the fragments (the nitronyl nitroxide and the metal fragment), using the structural results. The magnetic orbitals, Φ_A and Φ_B are found at -11.67 ev, each resulting from an interaction of the SOMO of one nitroxide with both the σ (-13.14 ev) and the σ^* (-11.31 ev) orbitals of the dirhodium fragment. In addition, there is a weak contribution of the π^* orbitals of the metal fragment lying at -12.07 ev. Therefore, these calculations show that the interaction between the SOMO's of the two nitroxides and the rhodium dimer moiety involves mainly the metal orbitals of σ symmetry. This result is in complete agreement with the experimental conclusions presented above.

In summary, a series of four adducts of rhodium trifluoroacetate dimer with nitroxyl free radicals have been prepared, and their structural and magnetic properties studied. Different nitroxyl–metal geometries and magnetic behaviors have been observed. Local symmetry considerations as well as extended Hückel calculations allow one to propose that the intramolecular internitroxyl coupling is mediated by the Rh–Rh bond and involves mainly a σ mechanism.

Registry No. **1**·C_6H_6, 119679-72-0; **2**, 111468-86-1; **3**, 111468-87-2; **4**, 111468-89-4; $Rh_2(tfac)_4$, 31126-95-1; Rh, 7440-16-6.

Supplementary Material Available: Tables of crystal data summary (Table SI), bond lengths and angles (Tables SII–IX), and anisotropic thermal parameters (Tables SX–XIII) (16 pages); tables of observed and calculated structure factors (Tables SXIV–XVIII) (62 pages). Ordering information is given on any current masthead page.

Kinetics and Mechanism of Phosphine Substitution for CO in $[Fe_2Co(CO)_9(CCO)]^-$

Stanton Ching and Duward F. Shriver*

Contribution from the Department of Chemistry, Northwestern University, Evanston, Illinois 60208. *Received September 12, 1988*

Abstract: Rate laws and activation parameters were determined for CO substitution of $[PPN][Fe_2Co(CO)_9(CCO)]$ by phosphine ligands. These results along with the dependence of the reaction on the nature of the incoming ligand support an associative mechanism. Previous NMR data indicate that the phosphines selectively attack the Co metal center. Activation parameters are $\Delta H^\ddagger = +7.2$ to $+10.3$ kcal/mol and $\Delta S^\ddagger = -34.0$ to -45.5 cal/mol K. The activated complex is proposed to attain an open structure by breaking either a metal–metal or metal–carbon bond. An increase in solvent polarity increases the rate of ligand substitution, whereas a change in the cation from PPN^+ to Me_4N^+ has a negligible effect. The rates of reaction were influenced by both the basicity and steric properties of the phosphines.

The reactions of molecular metal clusters present a mechanistic challenge because they are potentially more complex than reactions at single metal centers. An ensemble of metal atoms may undergo structural changes through modifications in both metal–metal and metal–ligand bonding.[1] Consequently, reactive sites and transition states can be difficult to determine. Metal–metal bonds are typically weak in comparison to metal–ligand bonds,[2] so cluster

(1) (a) Band, E.; Muetterties, E. L. *Chem. Rev.* **1978**, *78*, 639. (b) Evans, J. *Adv. Organomet. Chem.* **1977**, *16*, 319.

0002-7863/89/1511-3238$01.50/0